A&A 570, L14 (2014)
DOI: 10.1051/0004-6361/201425029


Astronomy & Astrophysics

Letter to the Editor

# The wonderful complexity of the Mira AB system⋆

S. Ramstedt[1], S. Mohamed[2], W. H. T. Vlemmings[3], M. Maercker[3], R. Montez[4], A. Baudry[5], E. De Beck[3], M. Lindqvist[3], H. Olofsson[3], E. M. L. Humphreys[6], A. Jorissen[7], F. Kerschbaum[8], A. Mayer[8], M. Wittkowski[6], N. L. J. Cox[9], E. Lagadec[10], M. L. Leal-Ferreira[11], C. Paladini[7], A. Pérez-Sánchez[12], and S. Sacuto[1]

[1] Department of Physics and Astronomy, Uppsala University, Box 516, 75120 Uppsala, Sweden
e-mail: sofia.ramstedt@physics.uu.se
[2] South African Astronomical Observatory, PO box 9, 7935 Observatory, South Africa
[3] Dept. of Earth and Space Sciences, Chalmers University of Technology, Onsala Space Observatory, 439 92 Onsala, Sweden
[4] Department of Physics & Astronomy, Vanderbilt University, Nashville, TN, USA
[5] Univ. Bordeaux, LAB, UMR 5804, 33270 Floirac, France
[6] ESO, Karl-Schwarzschild-Str. 2, 85748 Garching bei München, Germany
[7] Institut d'Astronomie et d'Astrophysique, Université Libre de Bruxelles, CP 226, Boulevard du Triomphe, 1050 Brussels, Belgium
[8] Dept. of Astrophysics, Univ. of Vienna, Türkenschanzstr. 17, 1180 Vienna, Austria
[9] Instituut voor Sterrenkunde, KU Leuven, Celestijnenlaan, 200D, 3001 Leuven, Belgium
[10] Laboratoire Lagrange, UMR 7293, Univ. Nice Sophia-Antipolis, CNRS, Observatoire de la Côte d'Azur, 06300 Nice, France
[11] Argelander-Institut für Astronomie, Universität Bonn, Auf dem Hügel 71, 53121 Bonn, Germany
[12] Centro de Radioastronomía y Astrofísica, Univ. Nacional Autónoma de Mexico, PO Box 3-72, 58090 Morelia, Mexico

Received 18 September 2014 / Accepted 3 October 2014

**ABSTRACT**

We have mapped the $^{12}$CO(3–2) line emission around the Mira AB system at 0.″5 resolution using the Atacama Large Millimeter/submillimeter Array (ALMA). The CO map shows amazing complexity. The circumstellar gas has been shaped by different dynamical actors during the evolution of the system, and several morphological components can be identified. The companion is marginally resolved in continuum emission and is currently at 0.″487 ± 0.″006 separation. In the main line component, centered on the stellar velocity, spiral arcs around Mira A are found. The spiral appears to be relatively flat and oriented in the orbital plane. An accretion wake behind the companion is clearly visible, and the projected arc separation is about 5″. In the blue wing of the line emission, offset from the main line, several large (~5–10″) opposing arcs are found. We tentatively suggest that this structure is created by the wind of Mira B blowing a bubble in the expanding envelope of Mira A.

**Key words.** stars: AGB and post-AGB – binaries: symbiotic – circumstellar matter – submillimeter: stars

## 1. Introduction

The Mira AB system is well-studied and nearby (the parallax distance is 92 pc, van Leeuwen 2007). It is a regularly pulsating M-type AGB star with a companion detected at 0.″6 separation (Karovska et al. 1997). The latest calculation of the orbit (Prieur et al. 2002) gives an inclination of 112°, an orbital period of ~500 yr, and the current separation is expected to be ~0.″5 with a position angle of ~100°. The mass-loss rate from Mira A is estimated to a few times $10^{-7}$ $M_\odot$ yr$^{-1}$ (e.g., Knapp et al. 1998; Ryde & Schöier 2001, without taking the asymmetries of the wind into account) and CO gas emission is detected with local-standard-of-rest (lsr) velocities from 37 to 54 km s$^{-1}$, which indicates a relatively low wind velocity (~5 km s$^{-1}$).

Several imaging studies have already shown the morphological intricacy of the circumstellar material on different scales. GALEX images revealed how interaction with the interstellar medium (ISM) has created a 2° tail and a bowshock ~3′ south of the system (Martin et al. 2007). They also show a series of knots on a 10′-scale, later studied in H$\alpha$ (Meaburn et al. 2009), and referred to as the north and south stream. The streams are tilted relative to the plane of the sky by 69° with the north part receding and the south approaching. On a somewhat smaller scale (~5′), *Herschel*/PACS imaged the cold dust (Mayer et al. 2011). The PACS images show the complex circumstellar dust distribution with several large arcs surrounding the system. Previous images of the CO emission show a wide bipolar structure with the north part approaching and the south receding (Planesas et al. 1990; Josselin et al. 2000; Fong et al. 2006), that is perpendicular to the north and south stream. The higher resolution (2.″5) map shows a 20″ butterfly shape where the molecular emission is believed to have been shaped by a low-velocity atomic outflow (Josselin et al. 2000). HST images first resolved the two stars and showed material flowing from Mira A to B (Karovska et al. 1997). This overflow was later confirmed by the *Chandra* X-ray image that shows a weak bridge between the two components (Karovska et al. 2005). It has been suggested that the accretion generates a wind from Mira B, which is confirmed by the P-Cygni profile of its strong Mg II *k* line (e.g., Wood & Karovska 2006). The wind is variable with mass-loss rates ranging from $5 \times 10^{-13}$ $M_\odot$ yr$^{-1}$ to $1 \times 10^{-11}$ $M_\odot$ yr$^{-1}$, and with terminal wind velocities observed between 250 km s$^{-1}$ and 450 km s$^{-1}$.

We have mapped the CO(3–2) line emission around the system with considerably higher spatial resolution than previous observations (~0.″5). In Sect. 2, we present the observations. In Sect. 3, the results are shown and interpreted. In Sect. 4, the

⋆ Appendix A is available in electronic form at http://www.aanda.org

morphology is set into the context created by previous observations, and possible shaping scenarios are discussed.

## 2. Observations

Mira was observed on 25 February 2014 with 27, and on 3 May 2014 with 30 of the main array 12 m antennas. It was also observed with seven Atacama Compact Array (ACA) 7 m antennas on 8 October 2013. The main array observations consist of a ten-point mosaic covering an area of $\sim 25'' \times 25''$. The same area is covered with three mosaic pointings with the ACA. The observations have four spectral windows with a width of 1.875 GHz (main array) and 2 GHz (ACA) centered on 331, 333, 343, and 345 GHz. The resulting spectral resolution is 0.488 MHz ($\sim$0.42 km s$^{-1}$) for the main array and ACA. The total time on source is 6.25 min with the main array and 6 min with the ACA. The baseline length of the main array ranges from 13 to 450 m, from which we find a maximum recoverable scale (MRS) of $\sim 6''$. The ACA covers 9 to 45 m baselines, and the MRS is $\sim 9''$. Calibration on the separate data sets was carried out using CASA, following standard procedures, using the quasar J0217+0144 as complex gain calibrator, quasars J0423-0120 and J006-0623 as bandpass calibrators, and Ganymede, Uranus and the quasar J0334-401 as flux calibrators. The data were subsequently combined, weighing the ACA data down by a factor of 0.3 to account for the lower sensitivity of the 7 m antennas. Tests indicate that the exact weight does not affect our results. A continuum image was made using the emission free channels from all spectral windows. Because the continuum emission is sufficiently strong, this image was used for self-calibration. After applying the self-calibration, final imaging was done after subtracting the continuum and averaging over two channels to $\sim$0.85 km s$^{-1}$ spectral resolution. The images have a beam full width half maximum (FWHM) of $0\farcs576 \times 0\farcs403$ and reach an rms noise of 23 mJy/beam in the emission-free channels.

## 3. Results

### 3.1. Continuum emission and current positions

The binary pair is marginally resolved when imaged in the continuum channels of the data (Fig. 2). The current positions determined by uv fitting (Martí-Vidal et al. 2014) are given in Table 1 together with the measured flux density at 338 GHz of the two sources. The separation is $0\farcs482 \pm 0\farcs005$ in right ascension (RA) and $0\farcs069 \pm 0\farcs003$ in declination (Dec). This gives a total separation of $0\farcs487 \pm 0\farcs006$. The flux density of Mira B fits the VLA radio continuum spectral index determination of Matthews & Karovska (2006) quite well, but that of Mira A is stronger by a factor of a few. For the $S_\nu \propto \nu^{1.5}$ relation determined by Matthews & Karovska (2006) for Mira A to hold to submm wavelengths, Mira A radio continuum must have become stronger by a factor $\gtrsim$4 since 2005.

### 3.2. Circumstellar morphology

The line profile is shown in Fig. 1 (left) and channel maps are presented in Appendix A. Comparison of our spectrum with previous single-dish observations (Young 1995) indicates that even with the ACA, only 50% of the extended flux is recovered. As a result, the channels with strong emission only reach a dynamic range (peak flux/S/N) of $\sim$50. The highly complex circumstellar morphology seen in the channel maps (Fig. A.1) has clearly been shaped by many different, probably interacting dynamical processes during the evolution of the system. Here we focus on the two most striking features: the large bubble-like structure found in the blue bump of the line (at $\sim$41.5 km s$^{-1}$, Figs. 1 and 3, left), and the spiral arcs (Fig. 3, right) found in the main line component centered on the stellar velocity at 47.0 km s$^{-1}$.

In the channel maps corresponding to the blue bump in the line profile, there is a large (5–10″) arc centered on Mira A and facing the companion. It grows with velocity and bends inward at the edges until, at $v_{\rm lsr}$ = 43.0 km s$^{-1}$, the gas forms a distinct bubble (Fig. 3, left) on the south-east side of Mira A. At higher velocities, the southern part becomes more noticeable until, beyond $v_{\rm lsr}$ = 44.5 km s$^{-1}$, other structures become more apparent. The edges of the bubble are sharp on the eastern (companion) side of Mira A, and no emission above the noise level of the observations is picked up inside the bubble, but, smooth, extended emission is resolved out (also when the ACA is used). Figure 1 (right) shows a position-velocity diagram created along the major axis (position angle 38°) of the southeastern bubble. It shows the slight velocity shift between the northern and southern part and that the northern part of the arc shifts from 2″ to 6″ offset from 39 to 44 km s$^{-1}$, indicating that part of the frontside of the bubble is visible at the velocities moving toward us. Although low surface brightness prevents detection at the extreme velocities at the very front- and back-side of the bubble, this gives a lower limit of the radial expansion velocity of $\sim$5 km s$^{-1}$.

Spiral arcs are seen from $v_{\rm lsr}$ = 45 to 54 km s$^{-1}$ (Fig. A.1). These channels make up the main part of the CO line profile and dominate the emission. At $v_{\rm lsr}$ = 47.5 km s$^{-1}$, the accretion wake behind the companion is apparent and is present through all redder velocity channels (Figs. 3 and A.2). The spiral can be traced out to two to three windings (Fig. A.2) and different parts are visible in different velocity channels, indicating that it is flatter and more confined to the orbital plane than the spiral around R Scl (Maercker et al. 2012), for instance. Since the orbital plane is inclined and seen close to edge-on (22° south of edge-on), the real winding separation cannot be determined directly from the map. The projected separation is about 3″–5″, which would correspond to 8″–13″, if the spiral is confined to the orbital plane.

## 4. Discussion

### 4.1. Comparison with previous observations

From the continuum emission (Sect. 3.1), the current position of Mira B is $\approx 0\farcs5$ east of Mira A at a position angle of 98°. This agrees with predictions from the orbit by Prieur et al. (2002).

The same north-south asymmetry as seen in previous CO observations is found in the ALMA CO line data; but because of the greatly improved spatial resolution and sensitivity, the ALMA data show much more detail. For instance, it is likely that the northeastern feature at 42.5 km s$^{-1}$ in the OVRO map (Planesas et al. 1990) is the large blueshifted arc detected with ALMA, but at low resolution. The butterfly shape found in the PdB map (Josselin et al. 2000) is not detected in the ALMA data, but it is possible that it is a low-resolution version of the structures seen in Fig. 3 (left). In the ALMA maps (Fig. A.1) there is no clear indication of the molecular gas being disrupted by a high-velocity outflow, as the one detected in KI emission (Josselin et al. 2000), or by the north and south stream.

It is not straightforward to connect the large dust arcs found in the PACS image (Mayer et al. 2011) and the inner spiral shape found in the ALMA data, since the dust distribution is affected by other processes. In addition, the PACS image only shows the

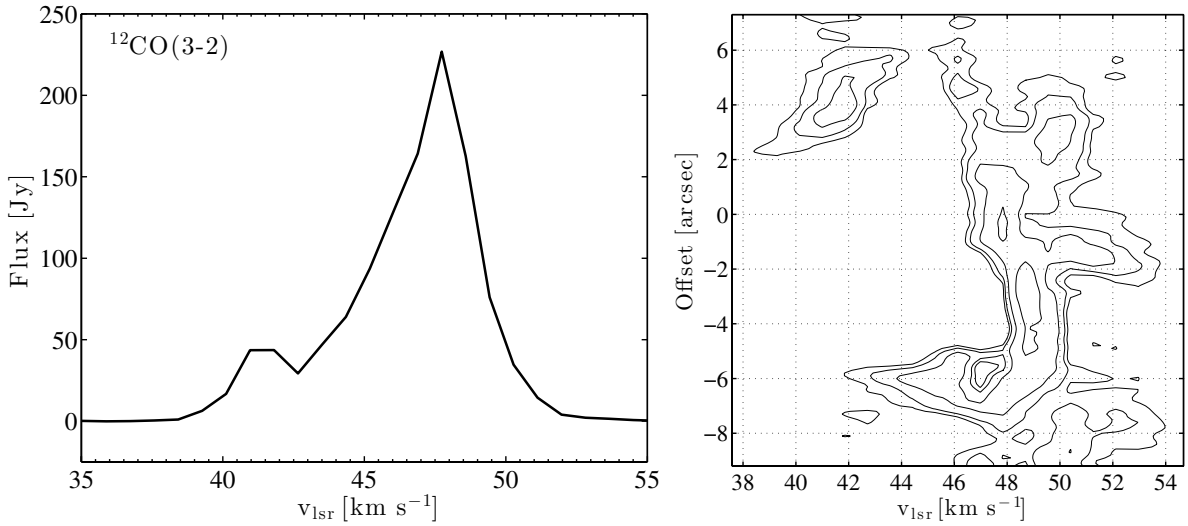


**Fig. 1.** *Left*: ALMA CO(3–2) line profile generated using an 25″ beam centered on Mira A. *Right*: position-velocity diagram showing the positional offset relative to the center of the bubble along a position angle of 38°, as a function of lsr velocity.

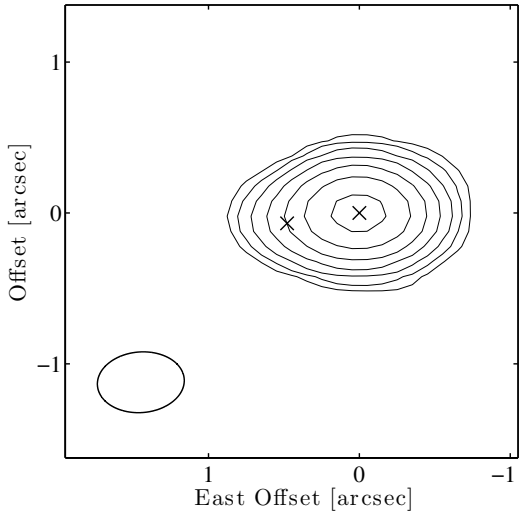


**Fig. 2.** Continuum emission at 338 GHz with the current positions of Mira A (west) and B (east, marked by crosses). The contours are drawn at 5, 10, 20, 40, 80, 160, and 320 times the rms noise level at 0.6 mJy/beam. The beam is shown in the lower left corner.

velocity-integrated information, and detailed structures may not be apparent (cf. PolCor and ALMA images of the spiral and shell around R Scl, Maercker et al. 2014). The separation between the dust arcs is about 15″–30″, which is significantly larger than in the inner spiral detected with ALMA.

Finally, the interaction between the circumstellar material and the ISM is seen in the GALEX images (Martin et al. 2007), and an extended bow shock is detected ≈5′ south of Mira AB. While the large-scale dust distribution is clearly shaped by this interaction (Mayer et al. 2011), this is not the case of the smaller-scale gas distribution mapped by ALMA. The presence of the bow shock much farther out means that the inner structures cannot be explained by (hydrodynamic) interaction with the ISM.

### 4.2. Possible shaping scenarios

The bubble found on the southeastern side of Mira A is ~800 AU across, and there is a similar, filled structure on the opposite, northwestern side of the star (Sect. 3.2 and Fig. 3, left). One possible explanation for these shapes is that the wind from Mira B is blowing a hole in the circumstellar envelope (CSE) of Mira A. The time scale for a continuous wind (assuming the higher Mira B mass-loss rate, $10^{-11}$ $M_\odot$ yr$^{-1}$, and wind velocity, 450 km s$^{-1}$, Wood & Karovska 2006) to create a bubble of that size is ~380 years (assuming $\dot{M}$ ~ $10^{-7}$ $M_\odot$ yr$^{-1}$ from Mira A). The terminal velocity of the shell surrounding the bubble would be ≈5 km s$^{-1}$ (e.g., the wind-wind interaction model for planetary nebulae, Kwok 1983). The bubble is not centered on Mira B because, in the direction of Mira A, the CSE is too dense to be significantly affected by the wind of Mira B. The wind will predominantly blow in the north-south direction since it is hindered by the (almost edge-on) dense accretion disk around Mira B, which might explain the bi-polar shape of the bubble. This scenario is consistent with the shell radial velocity of ≳5 km s$^{-1}$ (Fig. 1, right), and the mirrored shape on the opposite side of Mira A, which may have been created half a period ago. The northwestern bubble seems to be almost filled with material from the wind of Mira A, which agrees with the time scales and an expansion velocity of 5 km s$^{-1}$, but the time scale for the creation of the bubble from these order-of-magnitude estimates (assuming spherically symmetric winds) is slightly longer than the time Mira B would stay on either side of Mira A if the orbital period were 500 yr.

The two companions seem to be surrounded by a common dense molecular envelope, and at red-shifted velocities, there appears to be an accretion wake behind Mira B. Several arcs centered on Mira A are found in the line emission from 45.5 to 54.5 km s$^{-1}$ (Figs. 3, A.1 and A.2). Even though these arcs are physically connected in a continuous spiral, they will appear as separate arcs in velocity space, since different sections of the spiral arms will have different velocities along the line of sight. The relatively low wind velocity of Mira A (~5 km s$^{-1}$) will cause

**Table 1.** Current positions (ep = J2000.0) and continuum flux density at 338 GHz, $S_\nu$, of Mira A and B determined from the ALMA data.

| Source | RA | Dec | $S_\nu$ |
|---|---|---|---|
| Mira A | 02:19:20.784 | –02:58:42.818 | 252.3 ± 0.3 mJy |
| Mira B | 02:19:20.816 | –02:58:42.887 | 15.3 ± 0.3 mJy |

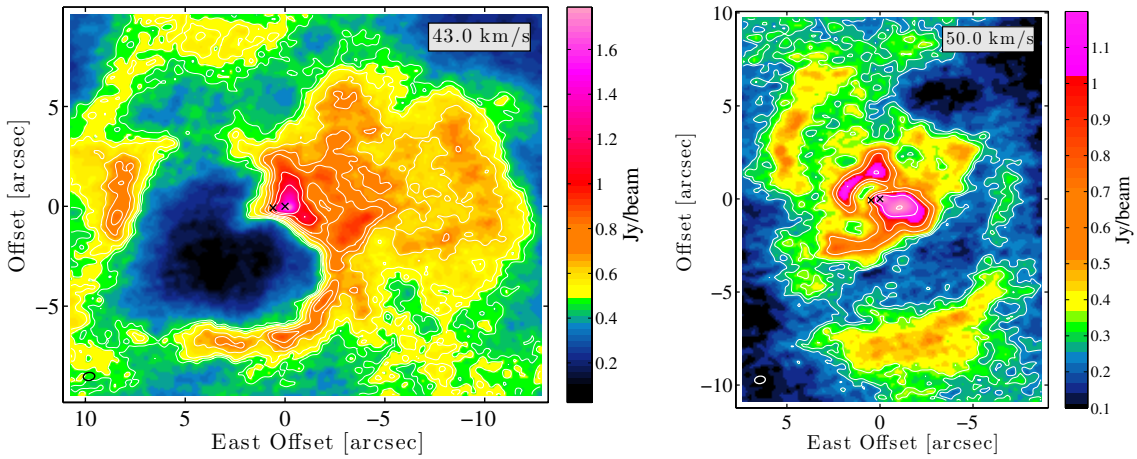


**Fig. 3.** CO(3–2) map averaged over 2 and 3 km s$^{-1}$ around $v_{\rm lsr}$ = 43.0 and 50.0 km s$^{-1}$, respectively, showing the bubble structure (*left*) and the spiral arcs (*right*) discussed in Sect. 3.2. The crosses mark the position of Mira A (west) and B (east). Contours are drawn at multiples of the rms noise level. The beam is shown in the lower left corner.

the circumstellar material to slowly fill its Roche lobe and eventually fall onto Mira B through the inner Lagrangian point (wind Roche-lobe overflow (WRLOF), Mohamed & Podsiadlowski 2007). This will focus the outflow toward the orbital plane, and the orbital motion will result in a rather flat spiral (Mohamed & Podsiadlowski 2012), unlike the case of R Scl for example (Maercker et al. 2012), where the AGB wind has a much higher expansion velocity (14.5 km s$^{-1}$) resulting in a spiral with greater vertical extension. Detailed modeling is beyond the scope of this paper and will be presented in a future publication. Preliminary results show that the spiral spacing will be on the order of 500–1000 AU or roughly 5″–10″ for a distance of 100 pc (assuming a gas outflow velocity of 5 km s$^{-1}$ and an orbital period between 500 and 1000 yr). The upper end of these theoretical estimates fit well within the observed spiral separation when we allow for orbital inclination effects.

## 5. Conclusions

The CO(3–2) emission from the Mira AB system has been mapped with ALMA in cycle 1. The maps show the circumstellar molecular gas distribution in amazing detail with the highest spatial resolution achieved so far. The complex morphology confirms that circumstellar material has been shaped by several interacting dynamical processes (e.g., mass loss, binary shaping, wind-wind interaction, accretion) during the evolution of the star, and the data presented here can be analyzed to better understand these processes.

The binary pair is marginally resolved in the continuum and has a separation of ≈0.″5 at a position angle of 98°. We suggest that the features seen in the CO gas emission confirm the scenario where the slow wind of the AGB star fills its Roche lobe and flows onto the companion in the orbital plane (Mohamed & Podsiadlowski 2007). A relatively flat spiral is formed and seen as separate arcs at different velocities. The spacing between the spiral arms agrees with what is expected from the orbit and wind properties of Mira A. The accretion of material onto the companion gives rise to a varying wind already detected in UV line emission (Wood & Karovska 2004). A tentative explanation is that this wind blows a large bubble in the circumstellar material as seen at slightly blueshifted velocities in the ALMA data. The wind from Mira B is pinched by the accretion disk and is therefore oriented preferentially in the north-south direction. Its flow is also confined by the dense wind of Mira A to the east. Our estimate of the radial velocity of the material in the shell around the bubble fits this scenario, while the time scale for the creation of the bubble is somewhat longer than the orbital period.

*Acknowledgements.* The authors would like to thank the staff of the Nordic ALMA ARC node for their indispensable help and support. This paper makes use of the following ALMA data: ADS/JAO.ALMA#2012.1.00524. S. ALMA is a partnership of ESO (representing its member states), NSF (USA) and NINS (Japan), together with NRC (Canada) and NSC and ASIAA (Taiwan), in cooperation with the Republic of Chile. The Joint ALMA Observatory is operated by ESO, AUI/NRAO and NAOJ. W.V. acknowledges support from Marie Curie Career Integration Grant 321691 and ERC consolidator grant 614264.

## References

Fong, D., Meixner, M., Sutton, E. C., Zalucha, A., & Welch, W. J. 2006, ApJ, 652, 1626
Josselin, E., Mauron, N., Planesas, P., & Bachiller, R. 2000, A&A, 362, 255
Karovska, M., Hack, W., Raymond, J., & Guinan, E. 1997, ApJ, 482, L175
Karovska, M., Schlegel, E., Hack, W., Raymond, J. C., & Wood, B. E. 2005, ApJ, 623, L137
Knapp, G. R., Young, K., Lee, E., & Jorissen, A. 1998, ApJS, 117, 209
Kwok, S. 1983, in Planetary Nebulae, ed. D. R. Flower, IAU Symp., 103, 293
Maercker, M., Mohamed, S., Vlemmings, W. H. T., et al. 2012, Nature, 490, 232
Maercker, M., Ramstedt, S., Leal-Ferreira, M. M. L., Olofsson, G., & Florén, H.-G. 2014 [arXiv:1409.4410]
Martí-Vidal, I., Vlemmings, W. H. T., Muller, S., & Casey, S. 2014, A&A, 563, A136
Martin, D. C., Seibert, M., Neill, J. D., et al. 2007, Nature, 448, 780
Matthews, L. D., & Karovska, M. 2006, ApJ, 637, L49
Mayer, A., Jorissen, A., Kerschbaum, F., et al. 2011, A&A, 531, L4
Meaburn, J., López, J. A., Boumis, P., Lloyd, M., & Redman, M. P. 2009, A&A, 500, 827
Mohamed, S., & Podsiadlowski, P. 2007, in 15th European Workshop on White Dwarfs, eds. R. Napiwotzki, & M. R. Burleigh, ASP Conf. Ser., 372, 397
Mohamed, S., & Podsiadlowski, P. 2012, Baltic Astron., 21, 88
Planesas, P., Bachiller, R., Martin-Pintado, J., & Bujarrabal, V. 1990, ApJ, 351, 263
Prieur, J. L., Aristidi, E., Lopez, B., et al. 2002, ApJS, 139, 249
Ryde, N., & Schöier, F. L. 2001, ApJ, 547, 384
van Leeuwen, F. 2007, A&A, 474, 653
Wood, B. E., & Karovska, M. 2004, ApJ, 601, 502
Wood, B. E., & Karovska, M. 2006, ApJ, 649, 410
Young, K. 1995, ApJ, 445, 872

Pages 5 to 6 are available in the electronic edition of the journal at http://www.aanda.org

## Appendix A:

Maps of the CO(3–2) emission from 36.7 to 53.7 km s$^{-1}$ at approximately 0.85 km s$^{-1}$ spectral resolution. As the maps with strong line emission are limited to a dynamic range of ~50 because a significant amount of large scale (>9″) flux is not recovered, the rms varies between 30 and 160 mJy in the different velocity channels.

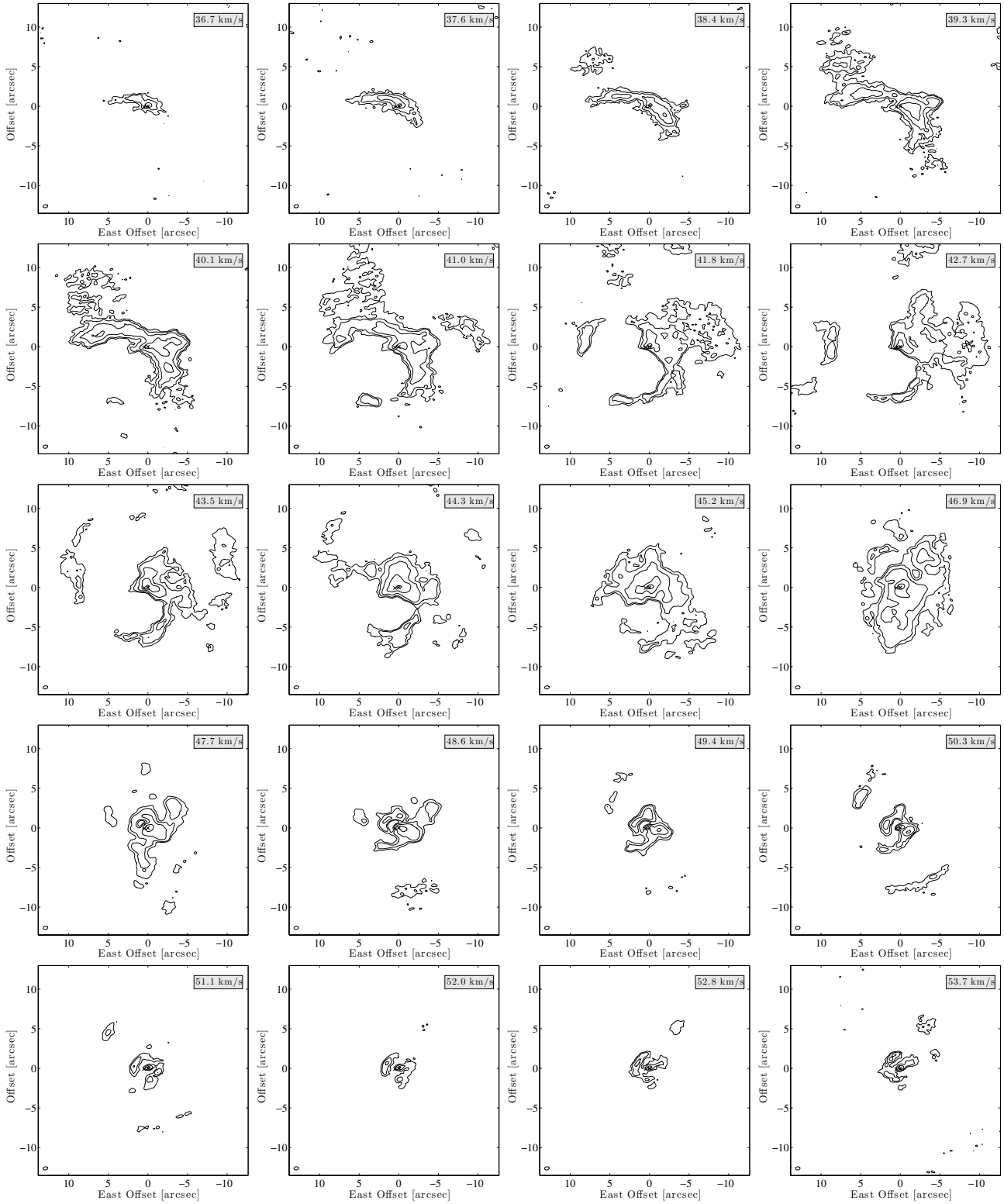


**Fig. A.1.** CO(3–2) map at 0.9 km s$^{-1}$ resolution. The crosses mark the positions of Mira A (west) and B (east). Contours are drawn at 3, 5, 10, 20, 40, and 80 times the rms noise level of the respective channel ranging from 30 to 160 mJy. The beam is shown in the lower left corner.

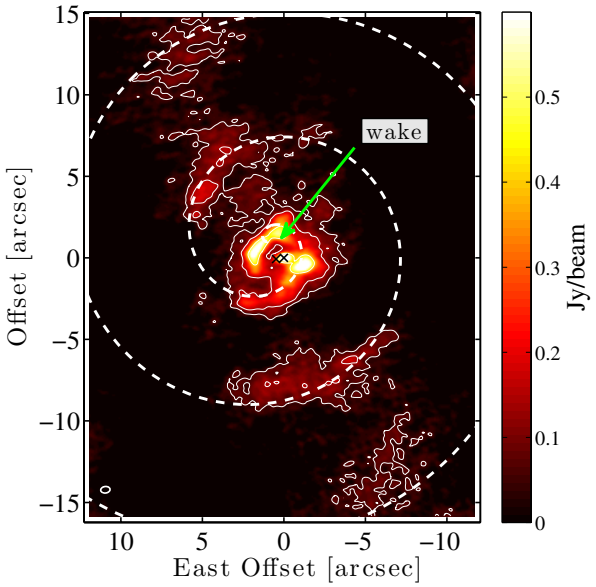


**Fig. A.2.** CO(3–2) map averaged from 49 to 54 km s$^{-1}$. The crosses mark the positions of Mira A (west) and B (east). Contours are drawn at 3, 5, 10, 20, 40, and 80 times the rms noise level of the respective channel ranging from 30 to 160 mJy. The beam is shown in the lower left corner. A spiral is overplotted to clearly mark the spiral windings, and the accretion wake behind the companion is indicated.

Figure A.2 shows an average from 49 to 54 km s$^{-1}$ where the spiral windings and the accretion wake discussed in Sects. 3.2 and 4.2 are clearly marked.